https://ntrs.nasa.gov/search.jsp?R=19930085269 2020-06-17T14:42:00+00:00Z

NACA TN 4367

NATIONAL ADVISORY COMMITTEE FOR AERONAUTICS

TECHNICAL NOTE 4367

WIND-TUNNEL TESTS OF A FULL-SCALE HELICOPTER ROTOR WITH SYMMETRICAL AND WITH CAMBERED BLADE SECTIONS AT ADVANCE RATIOS FROM 0.3 TO 0.4

By John L. McCloud III and George B. McCullough

Ames Aeronautical Laboratory
Moffett Field, Calif.

Washington
September 1958

NATIONAL ADVISORY COMMITTEE FOR AERONAUTICS

TECHNICAL NOTE 4367

WIND-TUNNEL TESTS OF A FULL-SCALE HELICOPTER ROTOR WITH SYMMETRICAL AND WITH CAMBERED BLADE SECTIONS AT ADVANCE RATIOS FROM 0.3 TO 0.4

By John L. McCloud III and George B. McCullough

SUMMARY

Wind-tunnel tests were made of a 44-foot-diameter, three-bladed helicopter rotor for the purpose of investigating the performance gains made available by delaying retreating blade stall by the use of blade sections with increased maximum lift. Marked changes in rotor-torque and blade pitching-moment characteristics afforded two means of defining stall boundaries of the rotor.

Comparison of these stall boundaries showed that the blades with cambered sections were superior to the blades with symmetrical sections in that the lifting capacity at a given forward speed was increased about 15 percent, or for equal lifts, forward speed capability was increased 20 to 25 percent.

For identical operating conditions within the capabilities of the rotor with symmetrical blades, the rotor with cambered blades required about 5 percent more power. Most of this increase probably was due to an upper surface irregularity on the cambered blades.

INTRODUCTION

The lifting capacity in forward flight and the maximum forward speed of helicopters are limited aerodynamically by stalling of the retreating rotor blades. Any method which increases the maximum lift and stalling angle of the blade sections could be expected to increase rotor performance capabilities. An obvious solution would be to use cambered, high-lift airfoil sections in the rotor blades. Although cambered sections have been employed in a few rotors, designers have, in general, used symmetrical sections because of their favorable high-speed and pitching-moment characteristics. In any case, direct comparisons of the forward flight capabilities of rotors employing symmetrical and cambered blade sections are lacking.

To determine whether the anticipated gains would be provided by the use of cambered blade sections, tests were made in the Ames 40- by 80-foot

wind tunnel. Stall boundaries were determined for a 44-foot-diameter, three-bladed helicopter rotor with two alternative sets of geometrically similar blades. One set of blades, which served as the basis of comparison, had symmetrical sections, and the second set had sections with a moderate amount of camber located well forward along the chord. Hereafter, these blades are referred to as symmetrical and cambered blades, respectively. Methods for determining stall boundaries were also investigated.

The tests were made in simulated forward flight corresponding to advance ratios of 0.3 to 0.4 with tip speeds of 450, 520, and 596 feet per second and blade-angle settings at the three-quarter radius station of 12°, 13°, 14°, and 15°.

Measurements were made of rotor force and moment characteristics. Blade flapping and lagging motion, and blade pitching moments were visually monitored and permanent records were taken.

Representative data are presented herein to show how the stall boundaries were determined, and these experimentally determined stall boundaries of the rotor with the two sets of blades are compared.

NOTATION

Positive directions of forces and moments are shown in the following sketches.

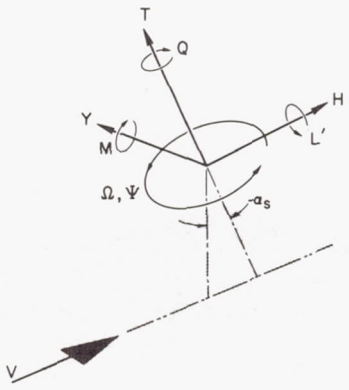

SHAFT AXES

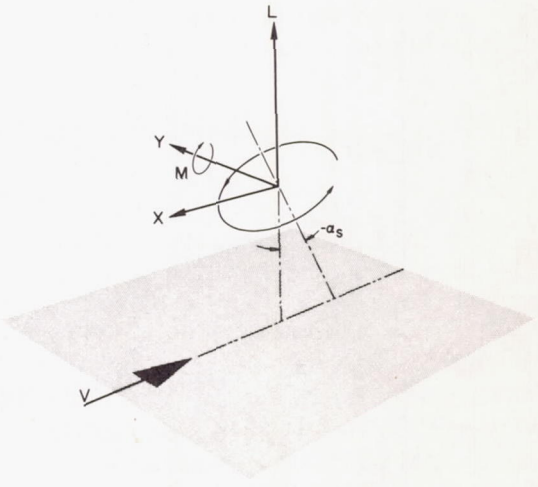

TUNNEL AXES

C_H in-plane drag coefficient, $\frac{H}{\rho(\Omega R)^2 \pi R^2}$

C_l rolling-moment coefficient, $\frac{L'}{\rho(\Omega R)^2 \pi R^3}$

C_L lift coefficient, $\frac{L}{q\pi R^2}$

C_{L_R} rotor lift coefficient, $\frac{L}{\rho(\Omega R)^2 \pi R^2}$

C_m pitching-moment coefficient, $\frac{M}{\rho(\Omega R)^2 \pi R^3}$

C_P power coefficient, $\frac{P}{\rho(\Omega R)^3 \pi R^2}$

C_Q torque coefficient, $\frac{Q}{\rho(\Omega R)^2 \pi R^3}$

C_T thrust coefficient, $\frac{T}{\rho(\Omega R)^2 \pi R^2}$

C_x longitudinal-force coefficient, $\frac{X}{q\pi R^2}$

C_Y lateral-force coefficient, $\frac{Y}{\rho(\Omega R)^2 \pi R^2}$

$\frac{V}{\Omega R}$ advance ratio

$\left(\frac{V}{\Omega R}\right)_{av}$ average value of advance ratio for a series of shaft angles

H in-plane drag force, lb

L lift force, lb

L' rolling moment, lb-ft

M	pitching moment, lb-ft
P	shaft power, lb-ft/sec
q	dynamic pressure, $\frac{1}{2}\rho V^2$, lb/sq ft
Q	shaft torque, lb-ft
R	rotor radius, ft
T	thrust force, lb
V	airspeed, ft/sec
X	longitudinal force, lb
Y	lateral force, lb
α_s	shaft angle, deg (equivalent to control axis inclination)
β	flapping angle, deg (positive up)
ζ	lagging angle, deg (positive for lag)
$\theta_{0.75}$	blade-section pitch angle; angle between line of zero lift of blade section and plane perpendicular to shaft axis measured at the 0.75 radius station, deg
ρ	mass density of air, slugs/cu ft
ψ	azimuth of blade measured counter-clockwise from downwind position, deg
Ω	angular velocity, radians/sec

APPARATUS

Rotor Support and Drive System

The rotor was supported in the wind tunnel by a tripod as shown in figure 1. The two lateral legs and the drive shaft were pivoted about a transverse axis beneath the tunnel floor. The extensible upstream leg was pivoted at both ends and could tilt the side legs and drive shaft 34° forward from the vertical by means of a motor-driven jackscrew. With the drive shaft vertical, the center of the hub was 20 feet above the

tunnel floor and 2 feet to the right of the center of the wind-tunnel passage (the advancing-blade side of the counterclockwise rotor). No windshields or fairings were provided to shield the rotor support from the air stream.

The rotor was driven by a variable-speed electric motor mounted rigidly beneath the tunnel floor. A bevel gear set in the speed reducer permitted the drive shaft to tilt forward about the same transverse axis as that of the lateral support legs.

Rotor Hub

The hub was fully articulated by means of offset flapping and lagging hinges. The flapping hinges were at 0.0174 radius (based on 44-feet diameter), and the lagging hinges at 0.0526 radius. To permit the blade pitch angle to change, the outer portion of each hub arm could rotate about its radial axis. The centrifugal tensile load of each blade was carried from this rotating member into the lagging hinge by a bundle of flat steel straps within the hub arm. Angular changes of blade pitch in either direction from a neutral position ($\theta_{0.75} = 8.7^\circ$) were resisted by the torsional action of the tension strap. The resistance was proportional to the blade angle and to the centrifugal tensile load. The orientation of the hinge axes was unaffected by blade pitch angle. The lagging motion was viscously damped. A sketch of the hub is shown in figure 2.

The usual helicopter collective- and cyclic-pitch controls were not employed; instead the rotor was operated with fixed blade angles, and the rotor attitude was changed by tilting the rotor drive shaft and side support legs. The blade-angle locking links and brackets can be seen in figure 3. Each link provided a turnbuckle type of adjustment for setting the blade pitch angles. To accommodate the large flapping angles relative to the drive shaft associated with tilting shaft operation, the flapping downstops were set to permit 12-1/2° of droop.

Rotor Blades

Two sets of blades were used; one set had symmetrical airfoil sections, and the other set had cambered airfoil sections with the camber positioned well forward along the chord similar to the NACA 230 series of airfoil sections. Both sets of blades were of the same general type of construction having a hollow steel spar which formed the forward one-third of an NACA 0012 airfoil section of 16-1/2-inch chord. The rear portion of each blade was formed by a series of 12-inch-wide aluminum boxes bonded to the rear of the spar. The chordwise contour of the boxes completed the airfoil section and trailing-edge tab.

The cambered blades differed from the symmetrical blades in that the camber was obtained by adding wood fairing strips to the forward portion of the basic symmetrical section. The addition of the wood fairing strips increased the basic chord of the cambered blades by approximately 3 percent, but the over-all chord length of the symmetrical blades was slightly greater than that of the cambered blades because of a longer trailing-edge tab. In the spanwise direction, the wood strips of the cambered blades were faired into an uncambered tip section along the outboard box. Also the trailing-edge tab did not extend into this box. The cambered blades also contained slots in the upper surface which extended from the 13-foot to the 21-foot radius station. These slots were covered by thin metal strips taped down with two layers of 0.009-inch-thick plastic tape which produced a small irregularity on the upper surface. Sketches of the blade plan form and the two blade sections are given in figure 4. Coordinates of the cambered section are given in table I.

Additional dimensions of the two rotors are given below:

	Rotor with symmetrical sections	Rotor with cambered sections
Solidity	0.065	0.064
Twist, deg	-7	-7
Weight per blade, lb	150	135
Radial station of c.g., in.	116	120

INSTRUMENTATION

The steady aerodynamic forces and moments were measured by the six-component wind-tunnel balance system. Rotor rotational speed was indicated by an electronic counter which measured the time for one revolution. The counter was pulsed by a stationary magnetically actuated switch adjacent to a permanent magnet attached to the drive shaft.

One arm of the hub was instrumented with potentiometers to give indications of the blade flapping and lagging motion.

The blade-angle locking links previously mentioned were provided with resistance-type strain gages to give indications of the moment about the blade pitch axis. The measured moment includes the aerodynamic moment of the blade, the centrifugal twisting moment of the blade, and the moment exerted by the tension strap. This total resultant moment is referred to as the blade pitching moment.

The electrical circuits for the hub instrumentation were led through a multiple-channel slip-ring assembly mounted on top of the hub (fig. 3),

and down through a nonrotating pipe inside of the hollow drive shaft. The indications were visually monitored during rotor operation, and permanent records were taken by a recording oscillograph. These data, however, are not complete or always accurate because of instrument difficulties encountered during the course of the test.

TEST PROCEDURE

When starting and stopping the rotor in the wind tunnel, it was deemed advisable to avoid operational regions in which retreating blade stall could be expected or which could impose overloads on the drive system. The rotor was started with the wind off and the shaft vertical and the wind speed and rotor speed increased together. Simultaneously, the shaft was tilted forward to the angle selected for the first data point (usually about -25° to -30°, depending on the blade pitch angle). Individual test runs were made with a substantially constant value of advance ratio $V/\Omega R$ with shaft angle as the test variable. Data were taken at selected values of shaft angle as the shaft was brought toward the vertical (the region of retreating blade stall). After some experience it was found that the blade pitching-moment trace as viewed on the scanning screen of the oscillograph provided a good indication of blade stall. The anticipated increase in support vibration or in the sound produced by the rotor did not provide a good indication of stall. Most test runs were terminated when two or three data points within the region of stall had been obtained.

Tests of the rotor with symmetrical blades were made at tip speeds of 450, 520, and 596 feet per second (195, 225, and 259 rpm, respectively). Since no effect of tip speed on the measured values of the rotor force and moment coefficients was observed within this speed range, tests of the rotor with cambered blades were made at a tip speed of 450 feet per second (195 rpm) to avoid the greater stresses associated with the higher speeds.

CORRECTIONS TO DATA

A few runs were made with the rotor removed to determine the force and moment contributions of the rotor support and slip-ring assembly. These support tares in coefficient form, which do not include the effect of rotor downwash on the support system, were removed from the gross data obtained with the rotor on. As would be expected, the longitudinal force tare (drag of the rotor support) was the largest in relative magnitude. For example, with a shaft angle of -18° and a tunnel dynamic pressure of 50 pounds per square foot the support tare drag coefficient based on rotor area was 0.0165, equivalent to a parasite-drag area of 25.1 square feet.

No tunnel-wall corrections were applied to the data because of the uncertainty of their validity. In any case, the presence or absence of full corrections should not affect the value of the data for purposes of comparing the relative performance capabilities of the two rotors. Blade pitching-moment data have not been corrected for tare changes with blade angle setting. These data are believed to be correct within ±200-inch-pound.

RESULTS AND DISCUSSION

A complete set of force and moment data for the rotor with symmetrical blades operated at nominal test conditions of 450 feet per second tip speed and 34 pounds per square foot dynamic pressure is shown in figure 5. These data are typical of all test conditions for the rotor with either set of blades in the following respects:

1. Variations of C_T, C_H, C_Y, and C_L with α_s are essentially linear.

2. As α_s is increased, C_X increases to a maximum and then decreases.

3. At shaft angles corresponding to high lift coefficients, there is a reflex in the C_Q curve.

In figure 6 are shown values of lift coefficient C_L from several different runs made with nominal tip speeds of 450, 520, and 596 feet per second plotted against advance ratio $V/\Omega R$. It can be seen that the effect of tip speed is negligible. The same was true for the other coefficients. Because of this lack of tip-speed effect, at least within the range employed in the present investigation, most of the subsequent data were obtained for a tip speed of 450 feet per second to lessen the possibility of structural damage to the rotor when operating in the region of retreating blade stall.

Determination of Retreating Blade Stall

Although stalling of the retreating blade is generally conceded to be the limiting factor in determining the maximum forward speed of a helicopter, it is known that a helicopter can fly with some amount of stall (e.g., ref. 1). It is probable that the amount of stall which can be tolerated depends on the particular helicopter under consideration. In general, then, the so-called stall boundaries, such as those described in references 1 and 2, do not constitute an exact limit to maximum forward

speed. For the purposes of comparing the two rotors of this report, the stall boundaries will be based on the first occurrence of retreating blade stall as indicated by the test data.

Indications of retreating blade stall.- In figure 5 it can be seen that the variations of forces and moments with shaft angle are reasonably smooth and continuous except for the torque coefficient, C_Q. The variation of C_Q shows an upturn commencing at a shaft angle of about -20° corresponding to the higher lift coefficients. It can be deduced that this upturn is an indication of rotor blade stall if one considers the total rotor torque to be the sum of three components: (1) the rotor profile torque (due to blade profile drag), (2) the rotor induced torque (due to lift), and (3) rotor propulsive torque (due to longitudinal force). In the absence of blade stall, the profile torque would be expected to be relatively independent of shaft angle, and hence to play a minor role in determining the shape of the total torque curve. In addition, for the range of advance ratios under consideration here, the rotor induced torque is a small part of the total torque and, hence, does not contribute much to the variation of the total torque with shaft angle. Therefore, the variation of the total torque (in the absence of blade stall) must be determined largely by the variation of the propulsive torque. This is borne out by the similarity between the total torque and the longitudinal force curves for shaft angles preceding the upturn of the total torque curve. Since the propulsive torque is diminishing for shaft angles beyond the upturn, the increase of total torque must be the result of an abrupt increase of profile torque such as would be caused by stalling of the retreating blades. On the basis of this criterion, data points beyond the upturn of the torque curve are believed to be in a region of retreating-blade stall and, as such, are represented by filled-in symbols. In order to define the boundary of this region, data were taken at closely spaced shaft angles as stall was approached. Figure 7 shows additional torque variations for the rotor with symmetrical and with cambered blades.

Further evidence of stall is given by the blade pitching-moment traces shown in figure 8(a). The upper two traces corresponding to shaft angles of -22° and -20° are reasonably smooth and continuous; whereas the trace for -19° is rough and shows a definite change in character for azimuth stations in the region from 270° to 0° (the region in which tuft studies have shown retreating blade stall to occur; e.g., ref. 1). Data points which correspond to irregular pitching-moment traces similar to the one shown are represented by flagged symbols to denote stall. In most cases, the agreement between the two criteria for determining stall was perfect so that symbols representing stall points shown in figures 5 and 7 are both filled and flagged. As previously mentioned, the pitching-moment trace as viewed on the scanning screen was used as the principal stall indicator during tunnel operation. Figures 8(b) and (c) show additional blade pitching-moment traces. For each blade angle, traces correspond to shaft angles believed to be just above and just below blade stall.

The blade-motion traces, examples of which are shown in figure 9, show only a progressive increase of the blade flapping and lagging motion as the shaft angle was increased in a positive direction into the region of stall. While harmonic analysis of the records might indicate the presence of stall, such a time-consuming process was not considered warranted.

Stall Boundary

By use of the previously described stall indicators, stall boundaries were determined for both sets of blades. To accomplish this, the lift coefficients C_L corresponding to the last point of unstalled operation and to the first point of stalled operation (unfilled and unflagged, and filled and flagged symbols, respectively) were plotted versus advance ratio $V/\Omega R$ in figure 10. It can be seen that the data fall into two fairly well-defined regions representing unstalled and stalled operation. The band drawn between these two regions is considered to be the stall boundary for the purpose of this report. The data points were obtained for the rotors with blade-angle settings $\theta_{0.75}$ of 12°, 13°, 14°, and 15°, but there was no systematic effect of blade angle on the location of the stall boundaries within this angle range.

Although the blade-angle setting had no significant effect on the rotor lift coefficient at the stall boundary, the data presented in figure 11 show that there was a pronounced effect of blade angle on the longitudinal force coefficient for the range of blade angles under consideration. In this figure, cross-plotted values of the longitudinal force coefficient C_X corresponding to rotor operation at the stall boundary are plotted against advance ratio $V/\Omega R$. It can be seen that at the stall boundary, the longitudinal force produced by either rotor can be varied over a fairly wide range by adjusting the blade angle. Since a helicopter in level flight with a parasite drag area f would require a value of C_X equal to $f/\pi R^2$, it is obvious then, that within the limits of C_X shown in figure 11, the stall boundary of a helicopter would be independent of fuselage drag.

The differences in the relationship between C_X and $V/\Omega R$ for the two rotors should not be interpreted as a superiority of one rotor over the other because at the stall boundary, the two rotors were operating at different values of lift and shaft angle. For this reason, a direct comparison of the two parts of the figure should not be made.

Comparison of the Two Rotors

The stall boundaries of figure 10 have been transposed in figure 12 as functions of rotor lift coefficient C_{L_R} (based on tip speed instead

of tunnel velocity) versus advance ratio $V/\Omega R$. Level flight then requires a constant value of this coefficient. The definite superiority of the rotor with cambered blades is readily apparent. Rotor lift at a constant advance ratio $V/\Omega R$ may be increased 13 to 15 percent, or, at constant lift and tip speed, forward speed may be increased 20 to 25 percent. For a helicopter whose payload is about 35 percent of its gross weight, the increased lifting capability would represent about a 40-percent increase in payload. The increased forward speed capability would be about 30 miles per hour for a rotor tip speed of 596 feet per second (the design value for the present rotor).

It may be seen by comparison of figures 8(b) and (c) that the blade pitching moments for the cambered blades were somewhat greater than for the blades with symmetrical sections. This is due in part to the fact that, for the conditions shows, the cambered blades are producing greater lift which would be reflected in the blade pitching moment because of the blade and hub geometry. In view of the absence of definite criteria for blade pitching moments it is impossible to assess the seriousness of the greater pitching moments of the cambered blades. Furthermore, a detailed analysis would be required for a particular control system.

Although the two rotors were operated at the same nominal values of tip speed and tunnel dynamic pressure, corresponding runs did not result in identical values of advance ratio $V/\Omega R$. Therefore, direct comparison of the data to detect small differences can not be made. To circumvent this difficulty some of the data were cross-plotted at identical values of $V/\Omega R$. Comparisons of the torque and propulsive force coefficients of the two rotors for a $V/\Omega R$ of 0.36 and blade angle $\theta_{0.75}$ of 14° are made in figure 13. For the same lift the longitudinal force of the two rotors is nearly identical, but the rotor with cambered blades required about 5 percent more power. Most of this power increment probably was due to the upper-surface irregularity on the cambered blades. The increased performance made possible by the cambered blades as shown in figure 10 would, of course, require additional power.

CONCLUDING REMARKS

A 44-foot diameter, three-bladed helicopter rotor provided with two alternative sets of blades having symmetrical and cambered sections has been investigated for a range of advance ratios from 0.3 to 0.4, to determine the effect of camber on retreating blade stall.

It was found that both rotor torque and blade pitching-moment characteristics provided readily discernible indications of blade stall. By use of these criteria, stall boundaries were determined and used to compare the maximum forward flight capabilities of the rotor with either

set of blades. On this basis, the rotor with cambered blades showed a definite superiority over the rotor with symmetrical blades in that:

1. The lifting capability at a given advance ratio was from 13 to 15 percent greater.

2. The forward speed capability for a given lift was 20 to 25 percent greater.

The power required by the rotor with cambered blades was about 5 percent greater at identical operating conditions. Most of this greater power requirement probably was due to an irregularity on the upper surface of the cambered blades.

Ames Aeronautical Laboratory
National Advisory Committee for Aeronautics
Moffett Field, Calif., July 25, 1958

REFERENCES

1. Gessow, Alfred, and Myers, Garry C., Jr.: Aerodynamics of the Helicopter. The Macmillan Co., N. Y., 1952.

2. Gessow, Alfred, and Tapscott, Robert J.: Charts for Estimating Performance of High-Performance Helicopters. NACA Rep. 1266, 1956. (Supersedes NACA TN's 3323 and 3482)

TABLE I.- COORDINATES OF THE CAMBERED BLADE SECTION

[Stations and ordinates given in percent of modified airfoil chord]

Station	Upper surface	Lower surface
0	0	0
1.25	2.35	-1.64
2.5	3.30	-2.17
5.0	4.67	-2.69
7.5	5.60	-2.98
10	6.22	-3.22
15	7.00	-3.58
20	7.38	-3.75
25	7.57	-3.93
30	7.57	-4.04
40	7.21	-4.17
50	6.46	-3.96
60	5.55	-3.49
70	4.41	-2.87
80	3.13	-2.11
90	1.71	-1.18
95	.93	-.67
100	.13	-.13
L.E. radius: 1.35-percent airfoil chord		

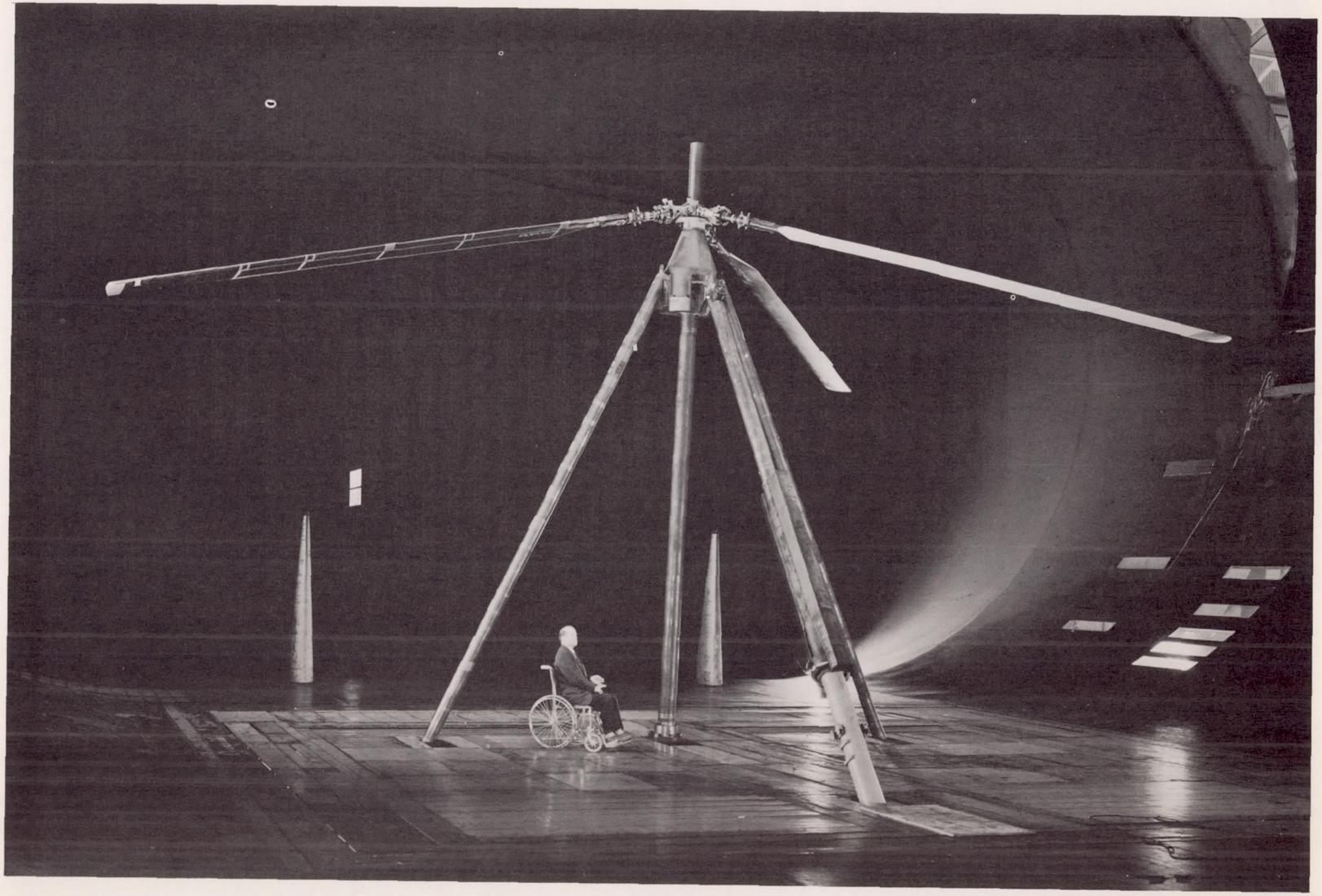

Figure 1.- Helicopter rotor and support mounted in wind tunnel.

A-22383

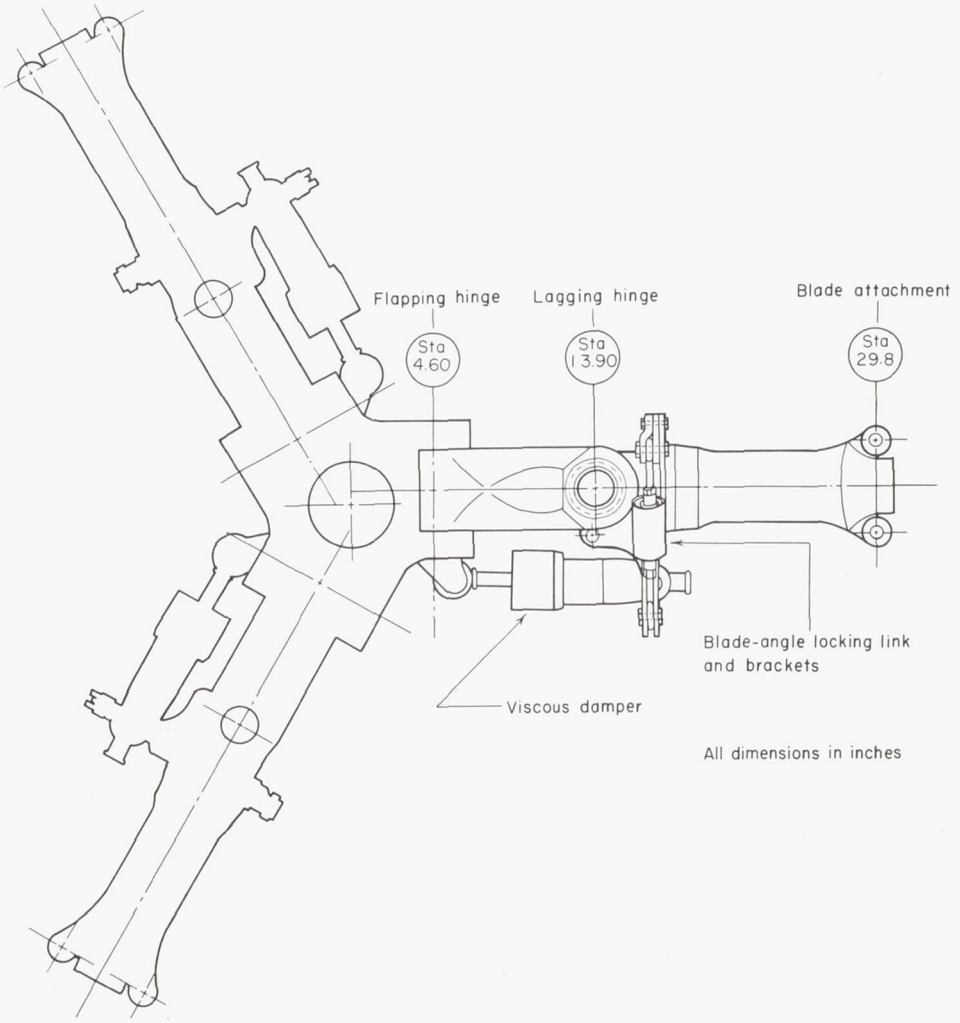

Figure 2.- Sketch of rotor hub.

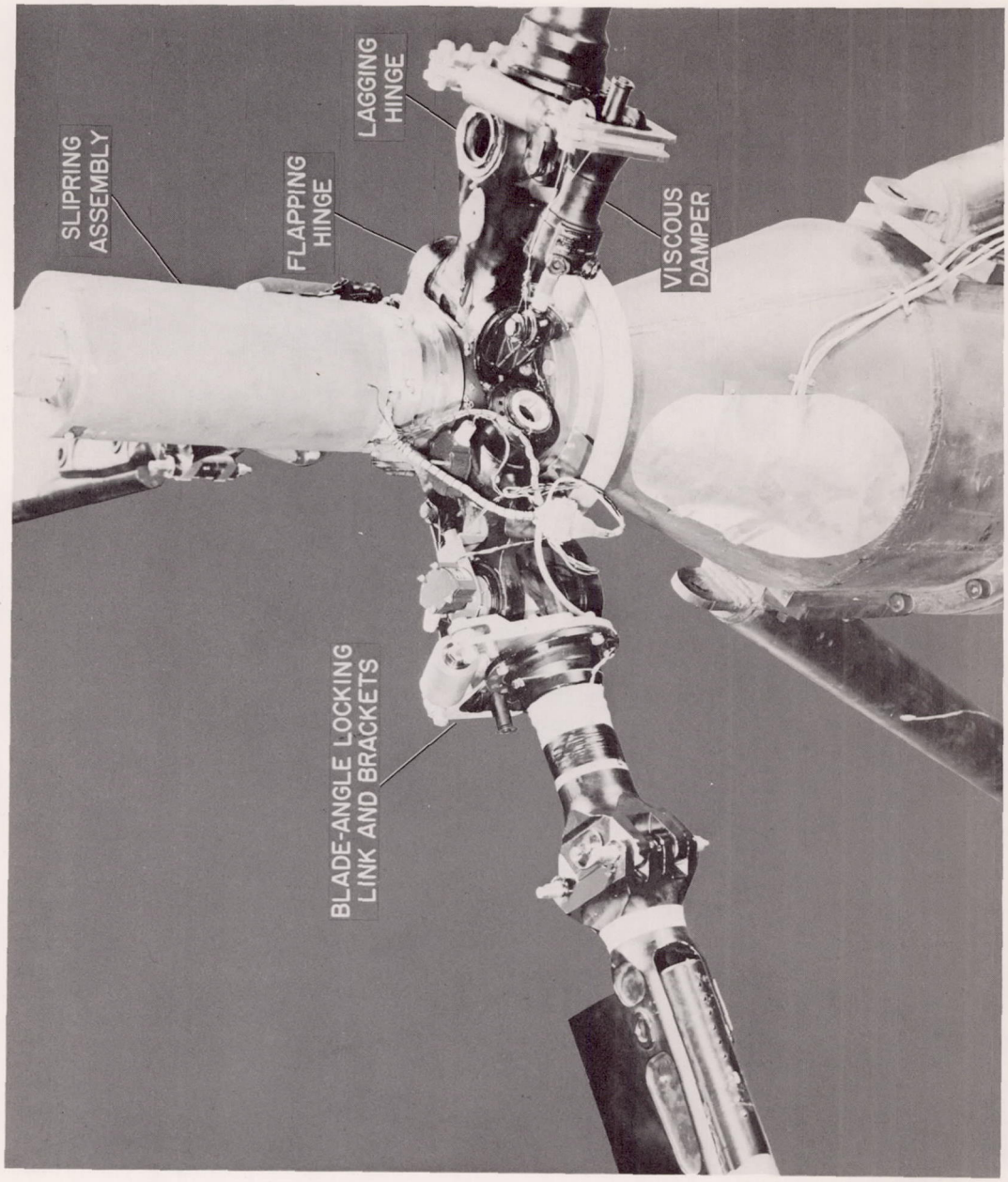

A-22763.1

Figure 3.- Photograph of rotor hub.

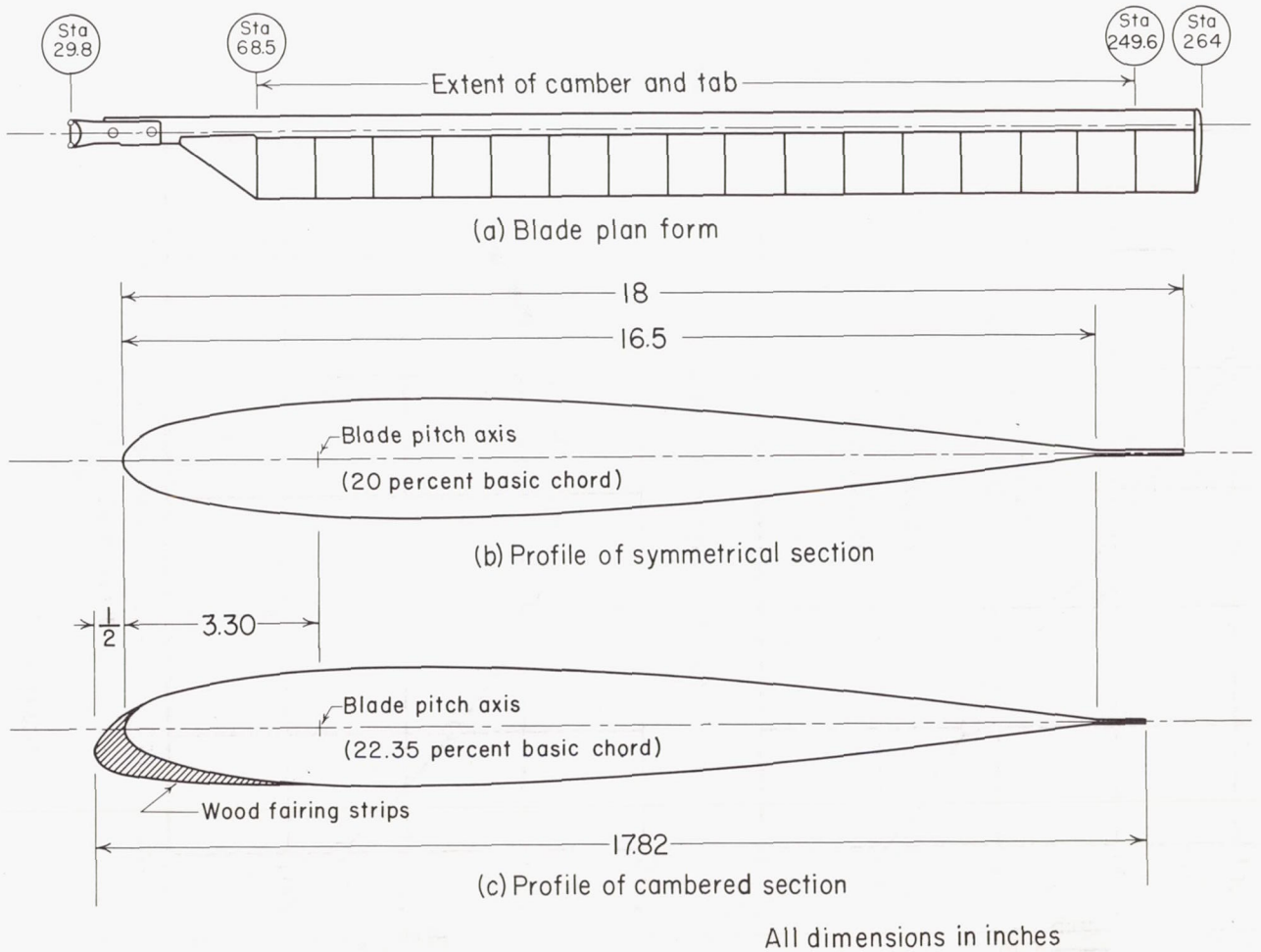

Figure 4.- Sketch of blade plan form and sections.

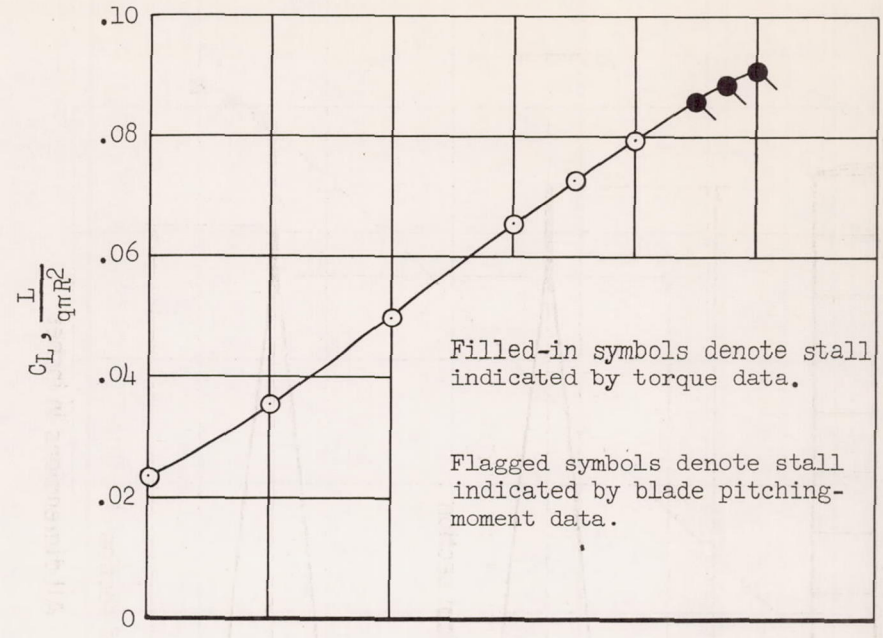

(a) Lift coefficient.

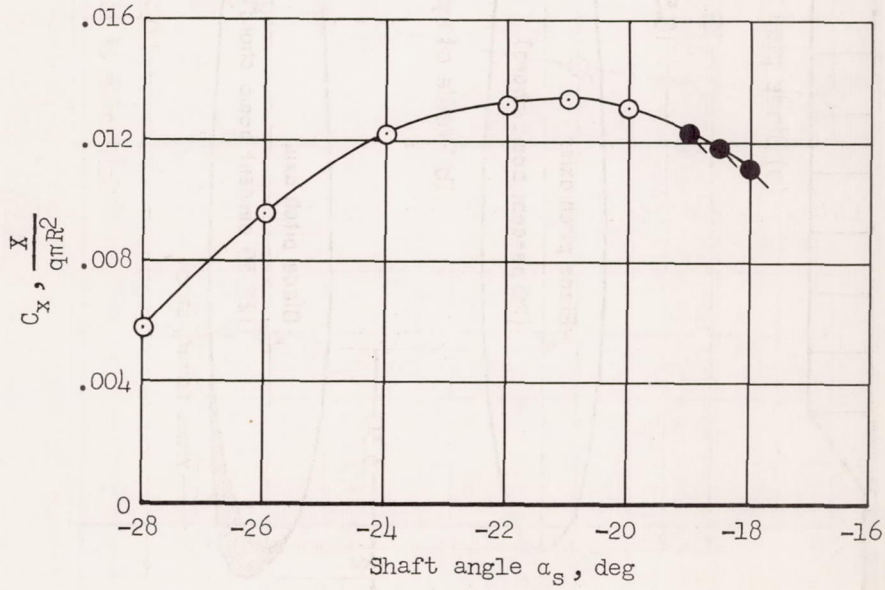

(b) Longitudinal-force coefficient.

Figure 5.- Typical aerodynamic force and moment characteristics of rotor with symmetrical blade sections; $\theta_{0.75} = 14^{\circ}$, tip speed = 450 feet per second; q = 34 pounds per square foot.

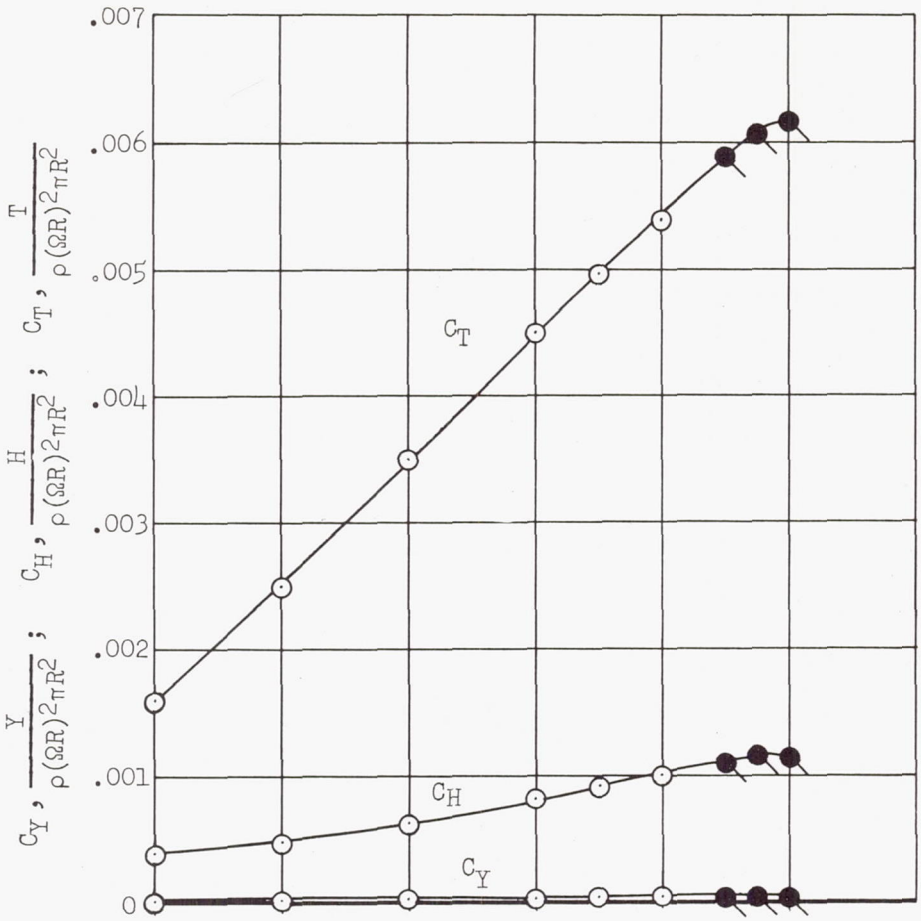

(c) Lateral-force, in-plane drag, and thrust coefficients.

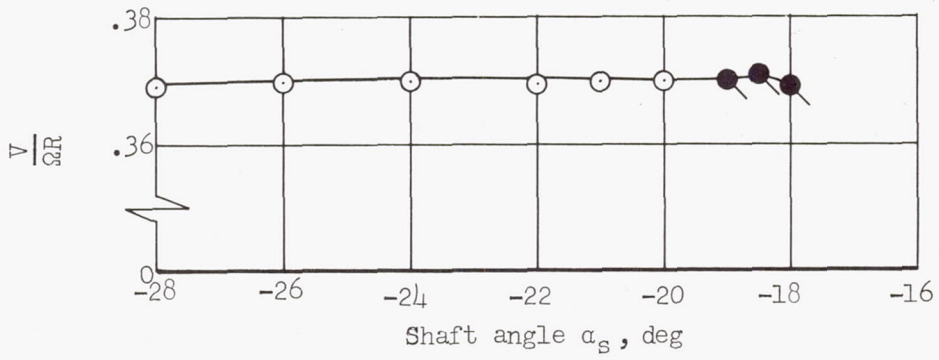

(d) Advance ratio.

Figure 5.- Continued.

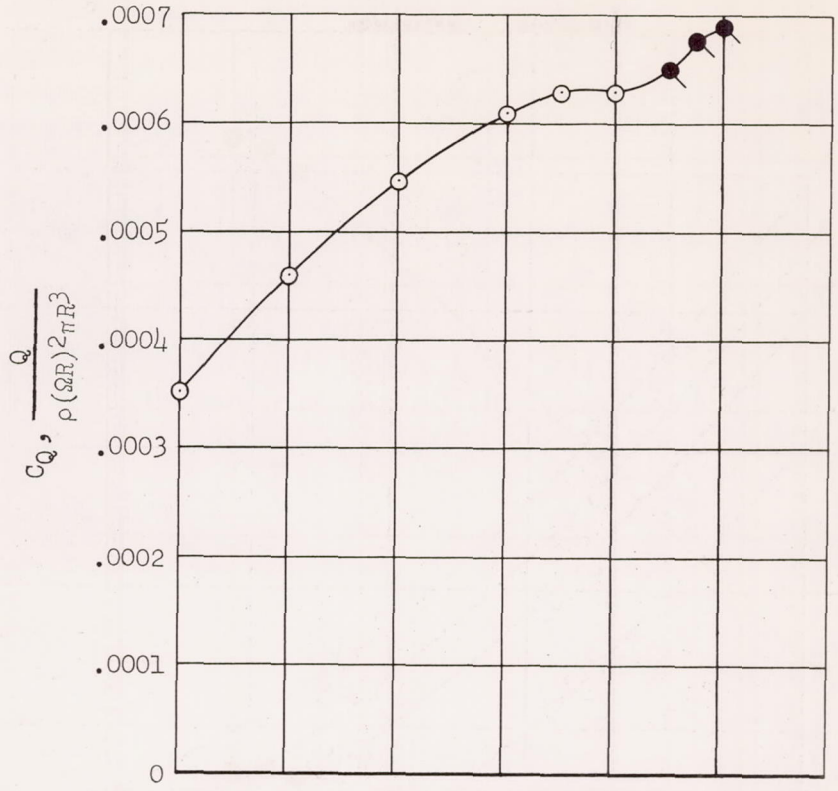

(e) Torque coefficient.

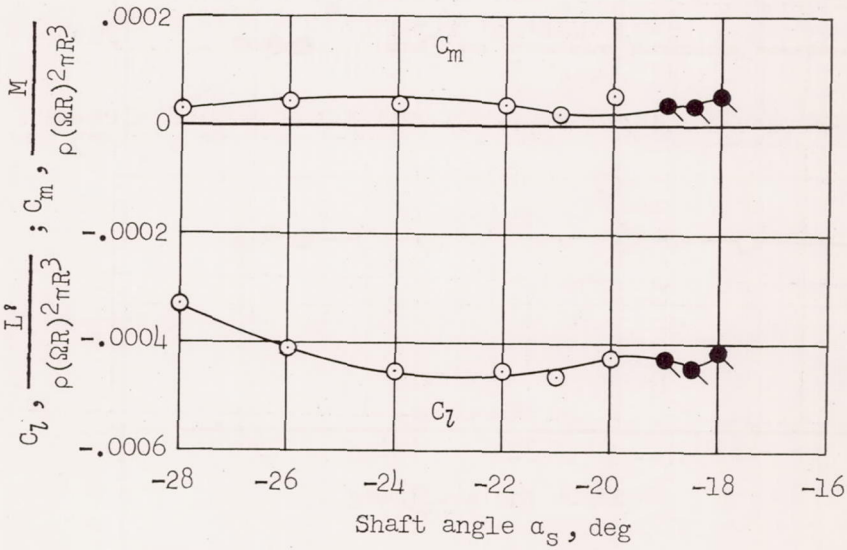

(f) Pitching-moment and rolling-moment coefficients.

Figure 5.- Concluded.

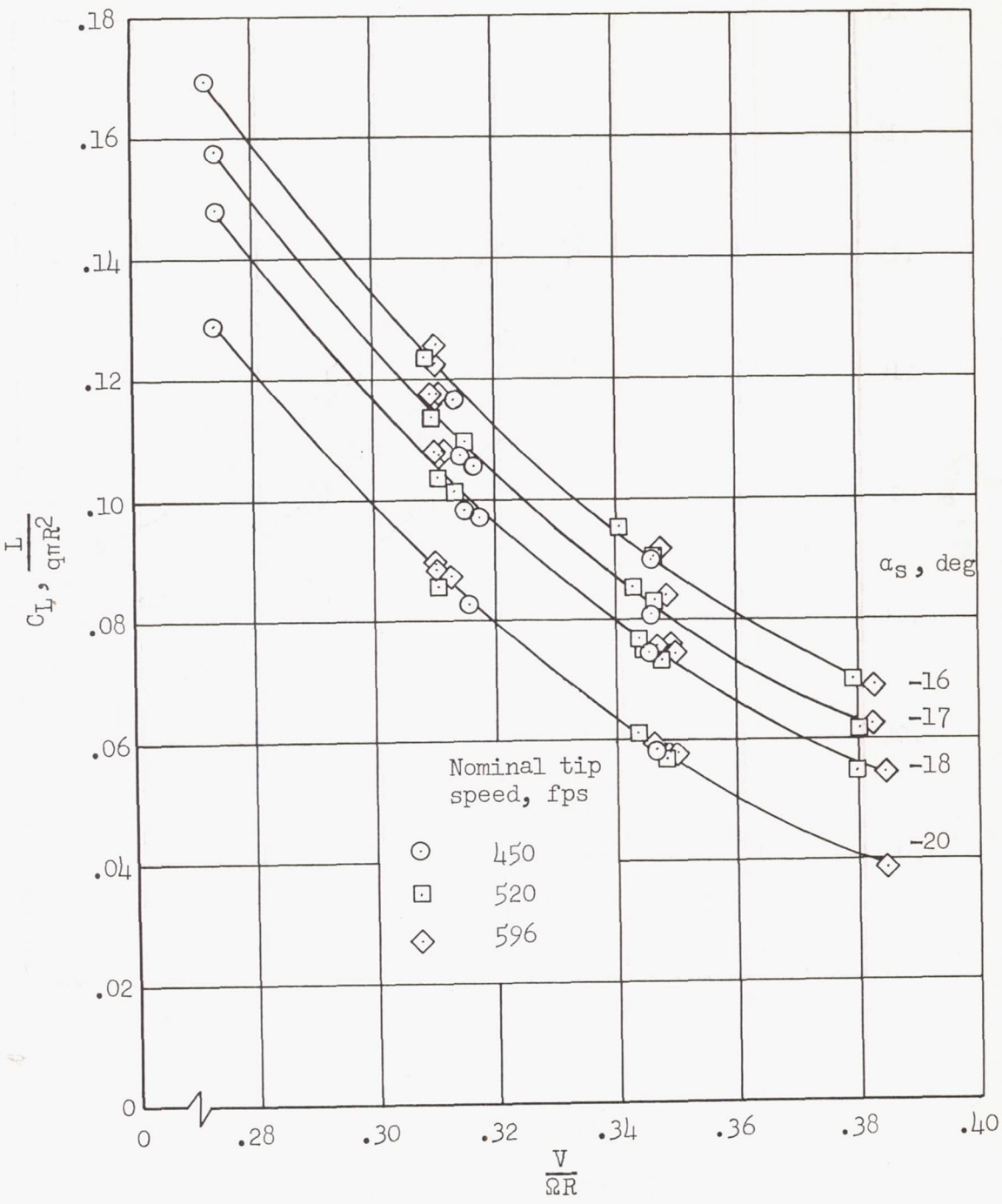

(a) $\theta_{0.75} = 12^\circ$

Figure 6.- Effect of tip speed for the rotor with symmetrical blade sections.

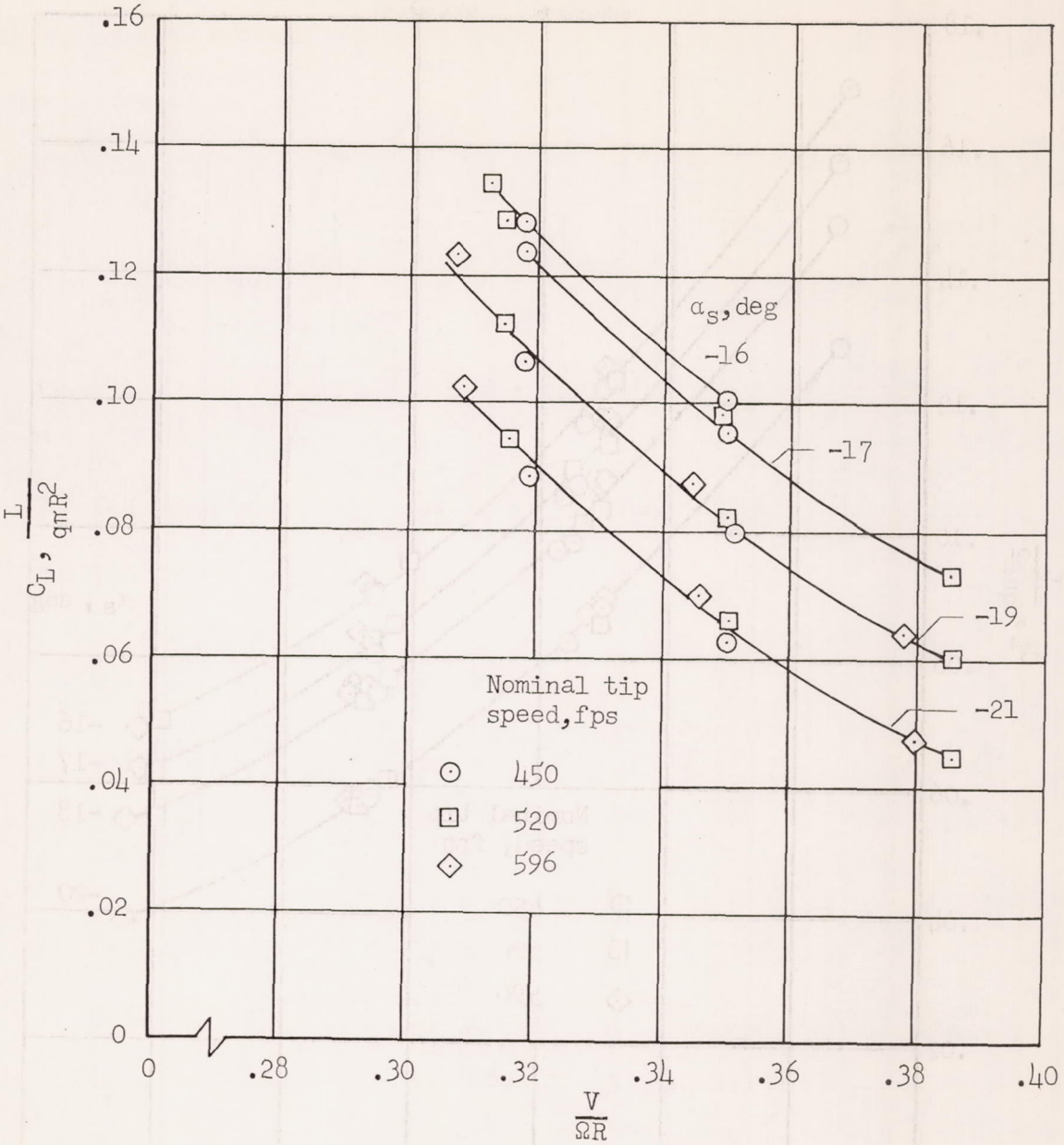

(b) $\theta_{0.75} = 13^\circ$

Figure 6.- Concluded.

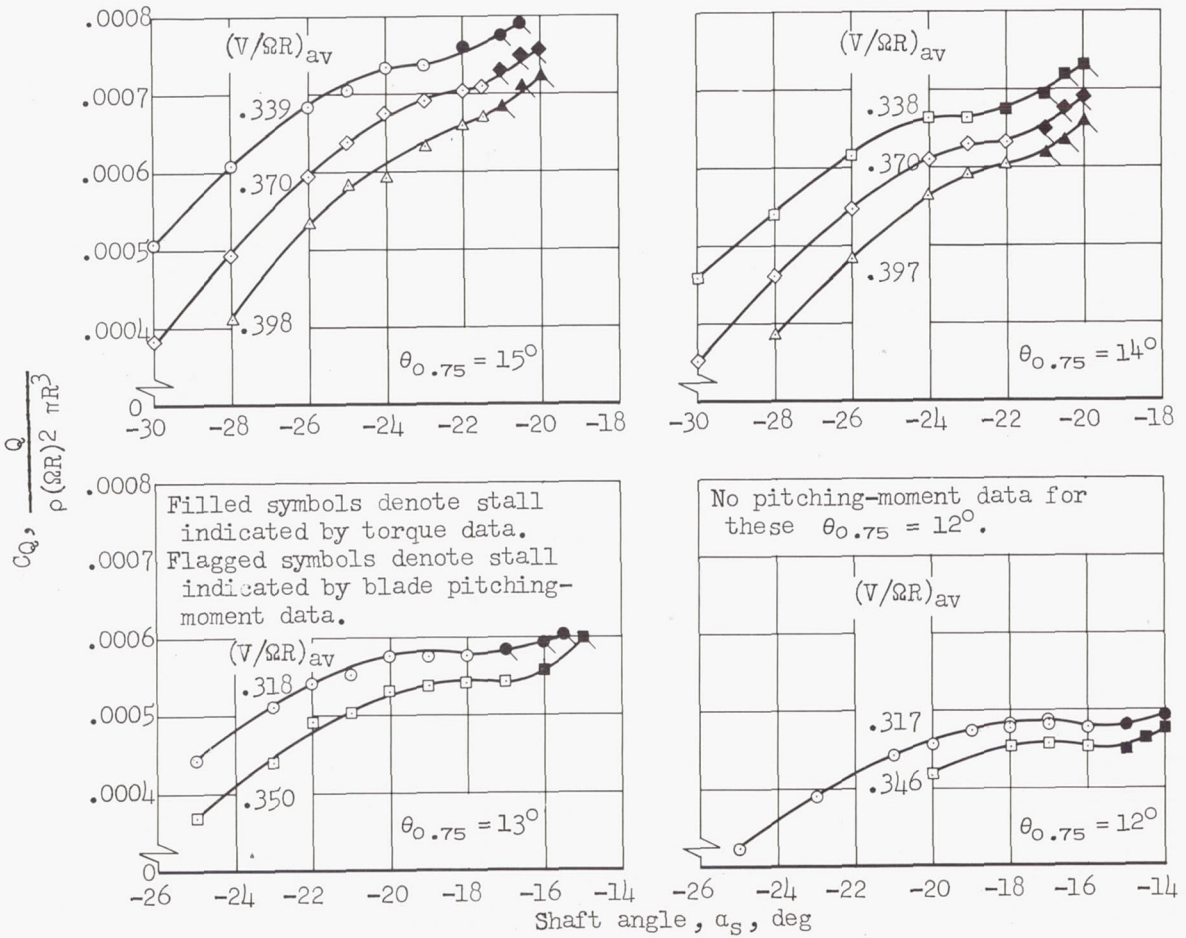

(a) Rotor with symmetrical blade sections.

Figure 7.- Examples of rotor torque variations used to define the stall boundaries; nominal tip speed = 450 feet per second.

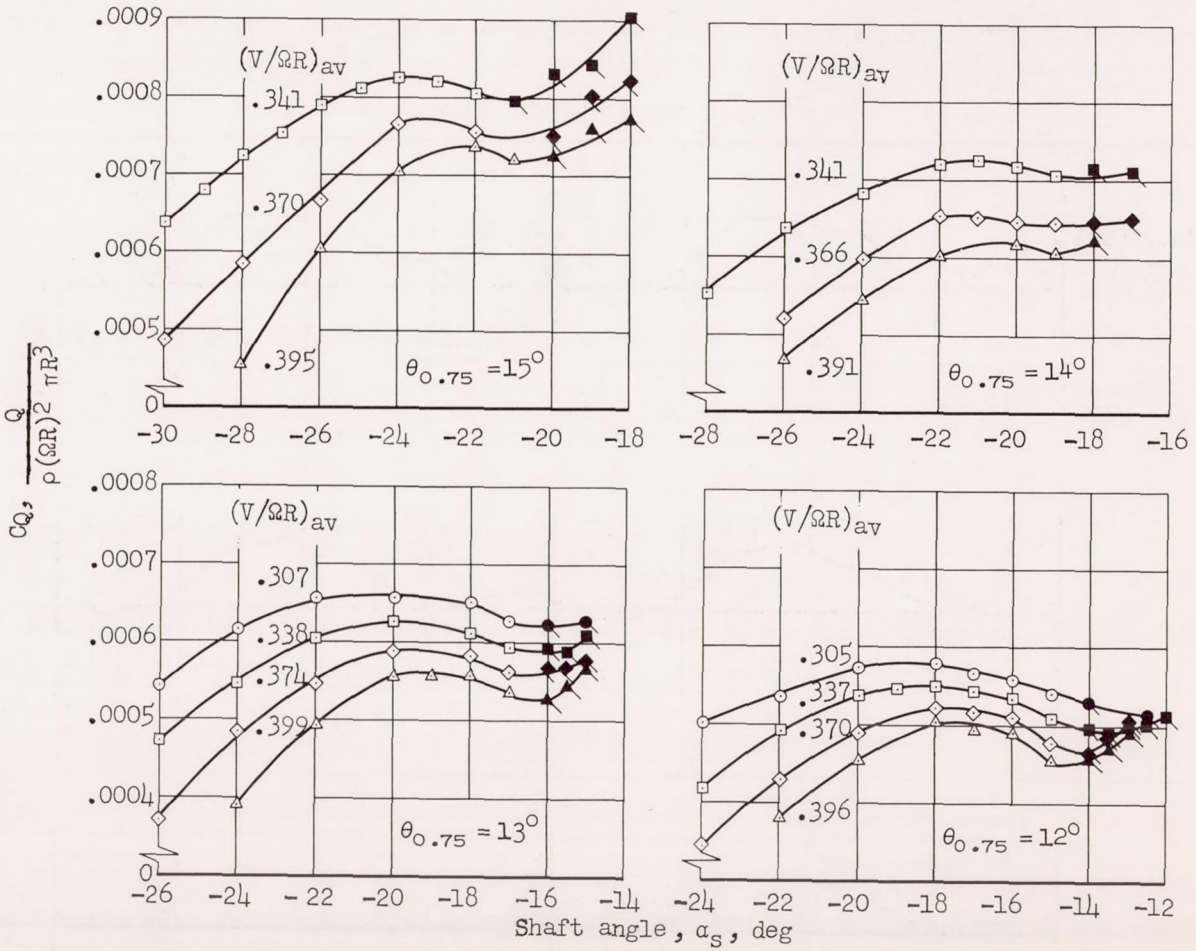

(b) Rotor with cambered blade sections.

Figure 7.- Concluded.

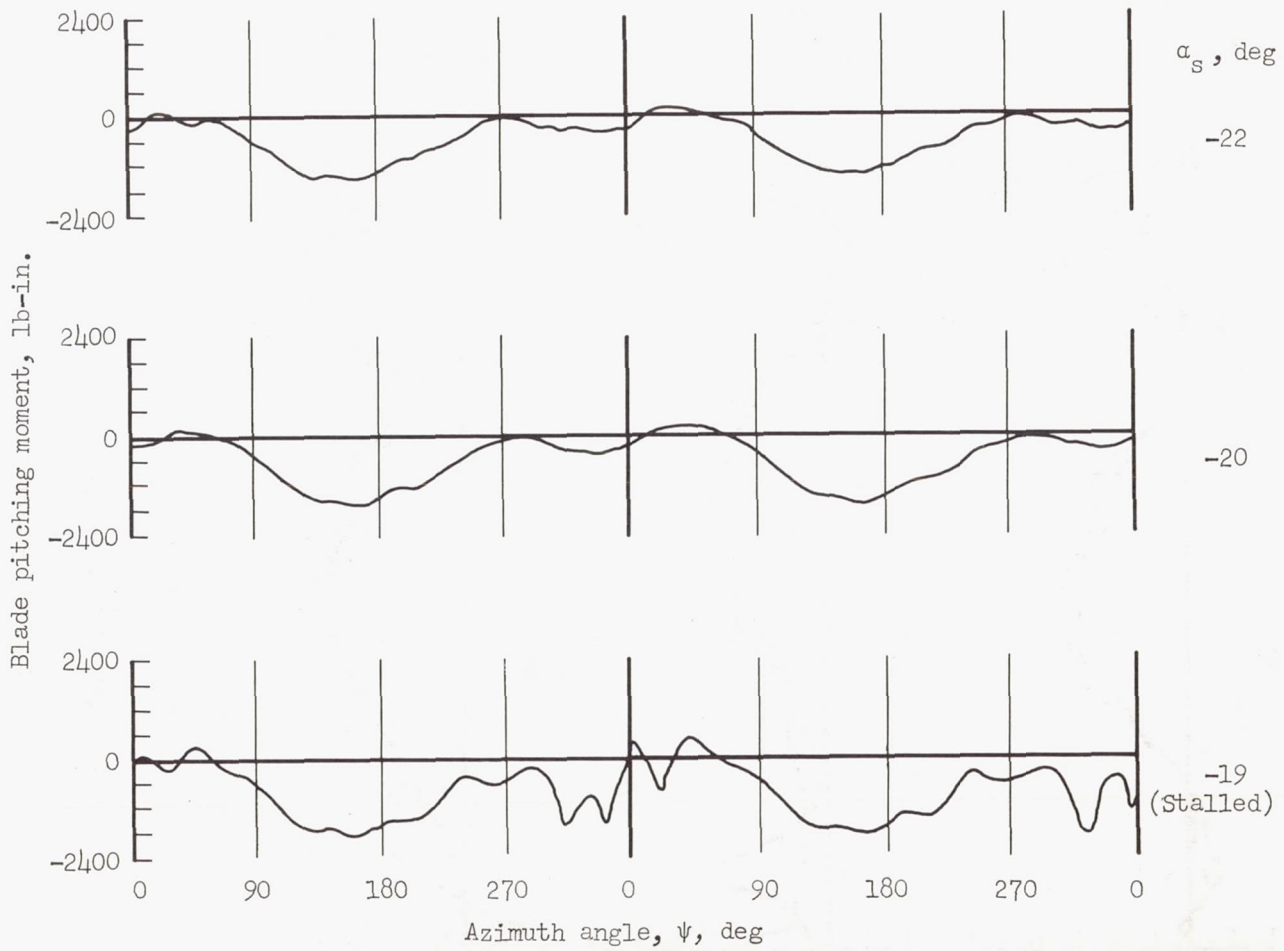

(a) Rotor with symmetrical blade sections; $\theta_{0.75} = 14^{\circ}$; $(V/\Omega R)_{av} = 0.370$.

Figure 8.- Typical blade pitching-moment traces; nominal tip speed = 450 feet per second.

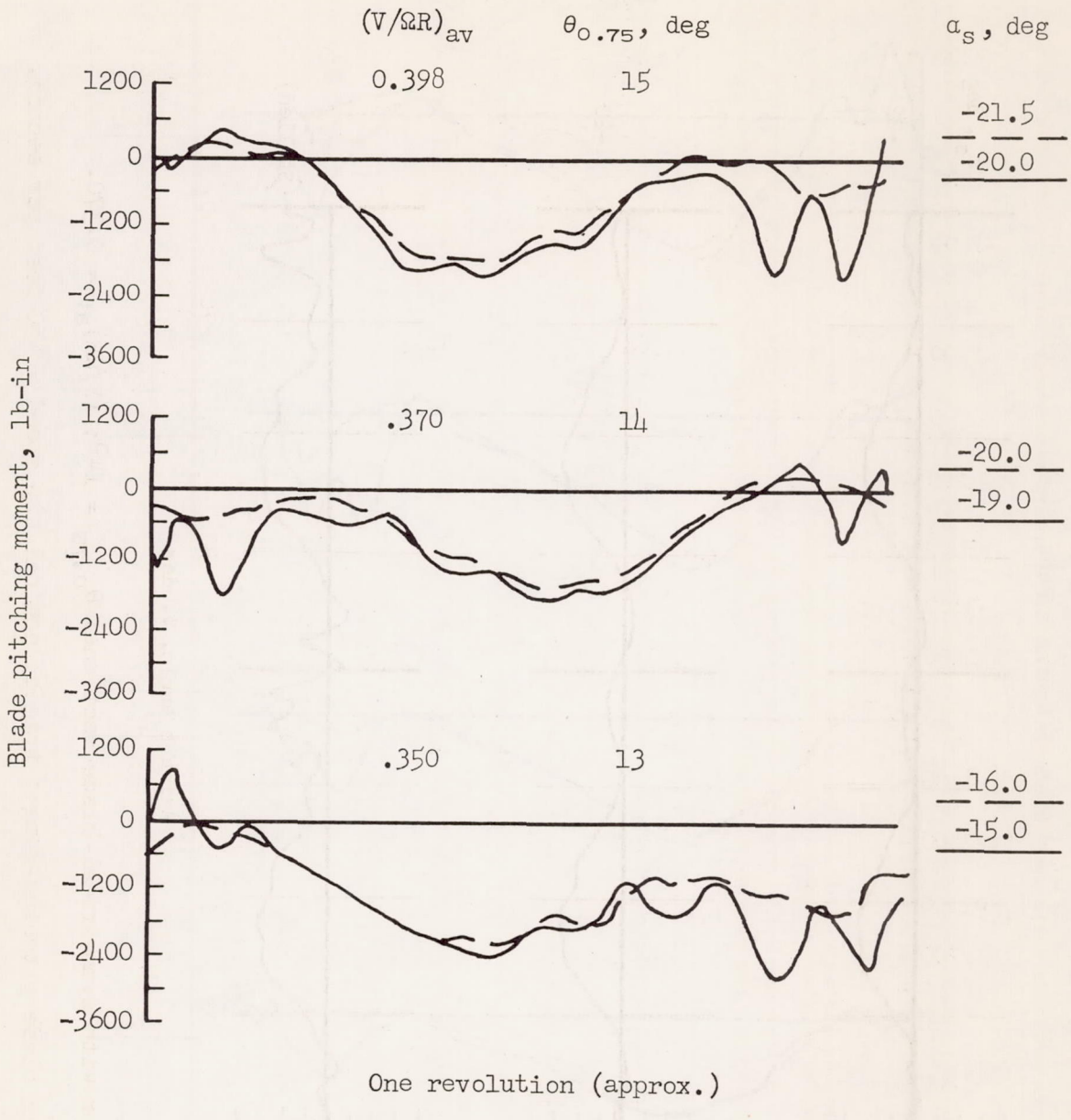

(b) Rotor with symmetrical blade sections.

Figure 8.- Continued.

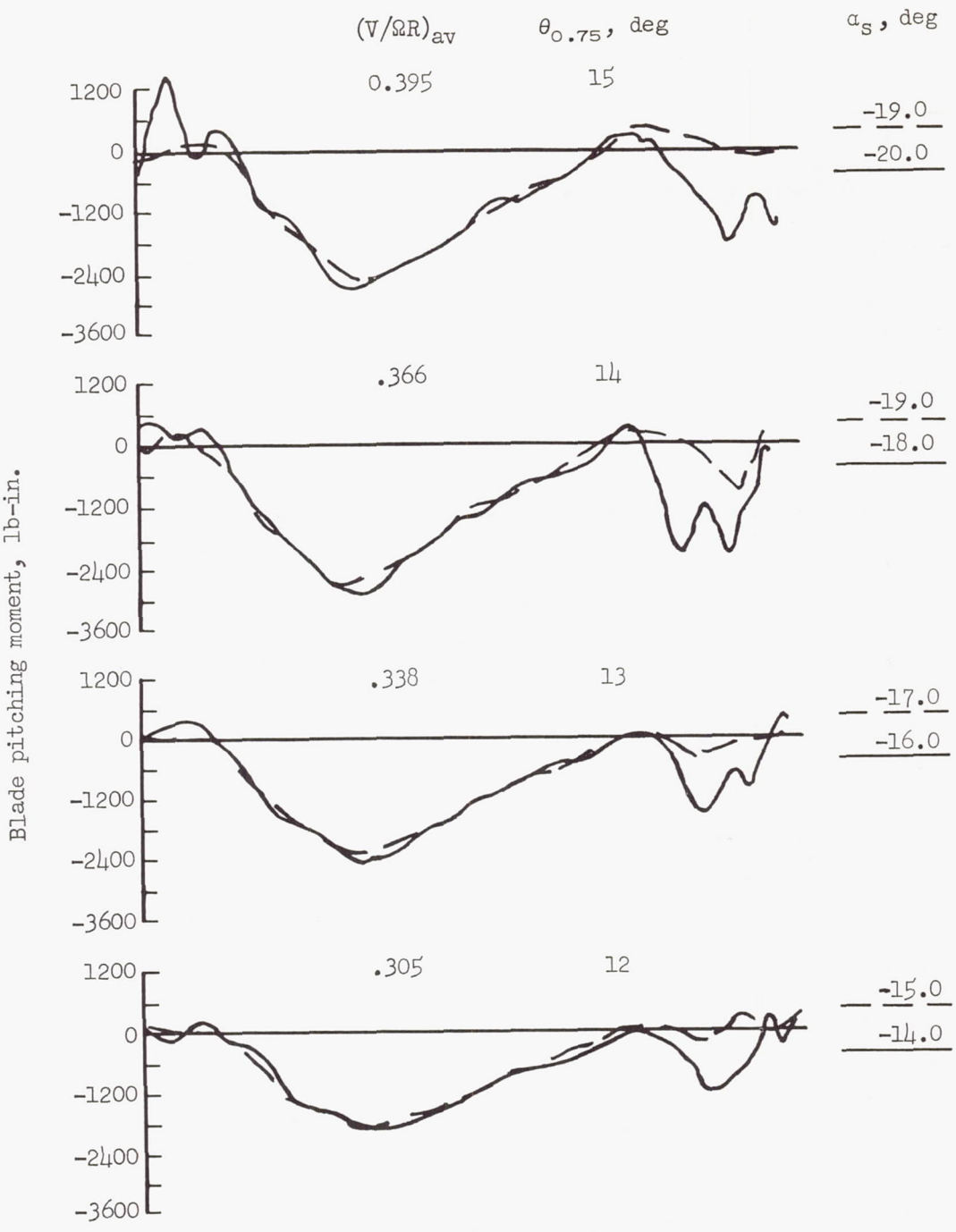

(c) Rotor with cambered blade sections.

Figure 8.- Concluded.

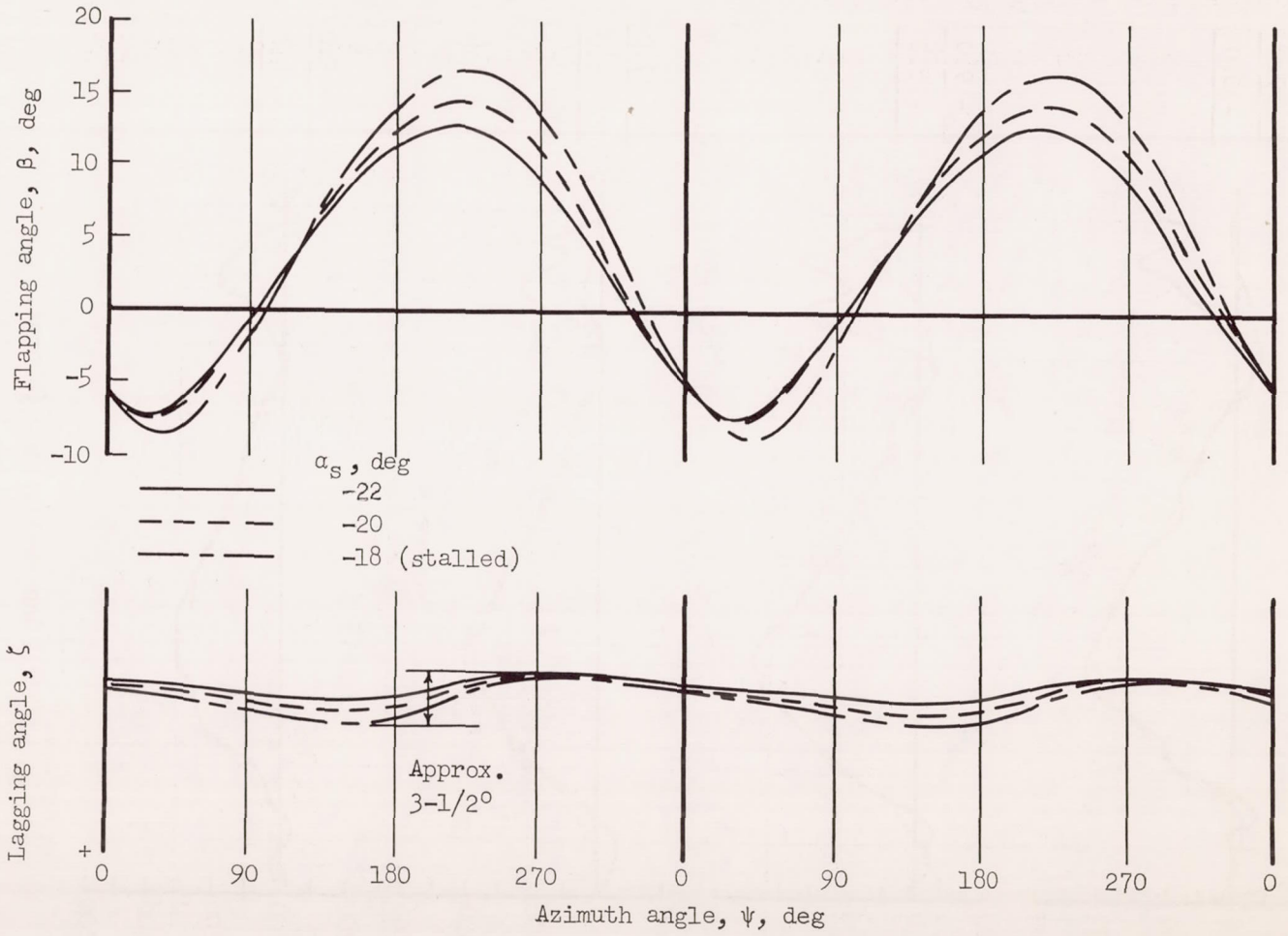

Figure 9.- Examples of rotor blade motion traces for the rotor with symmetrical blades; $\theta_{0.75} = 14^{\circ}$; nominal tip speed = 450 feet per second; q = 34 pounds per square foot.

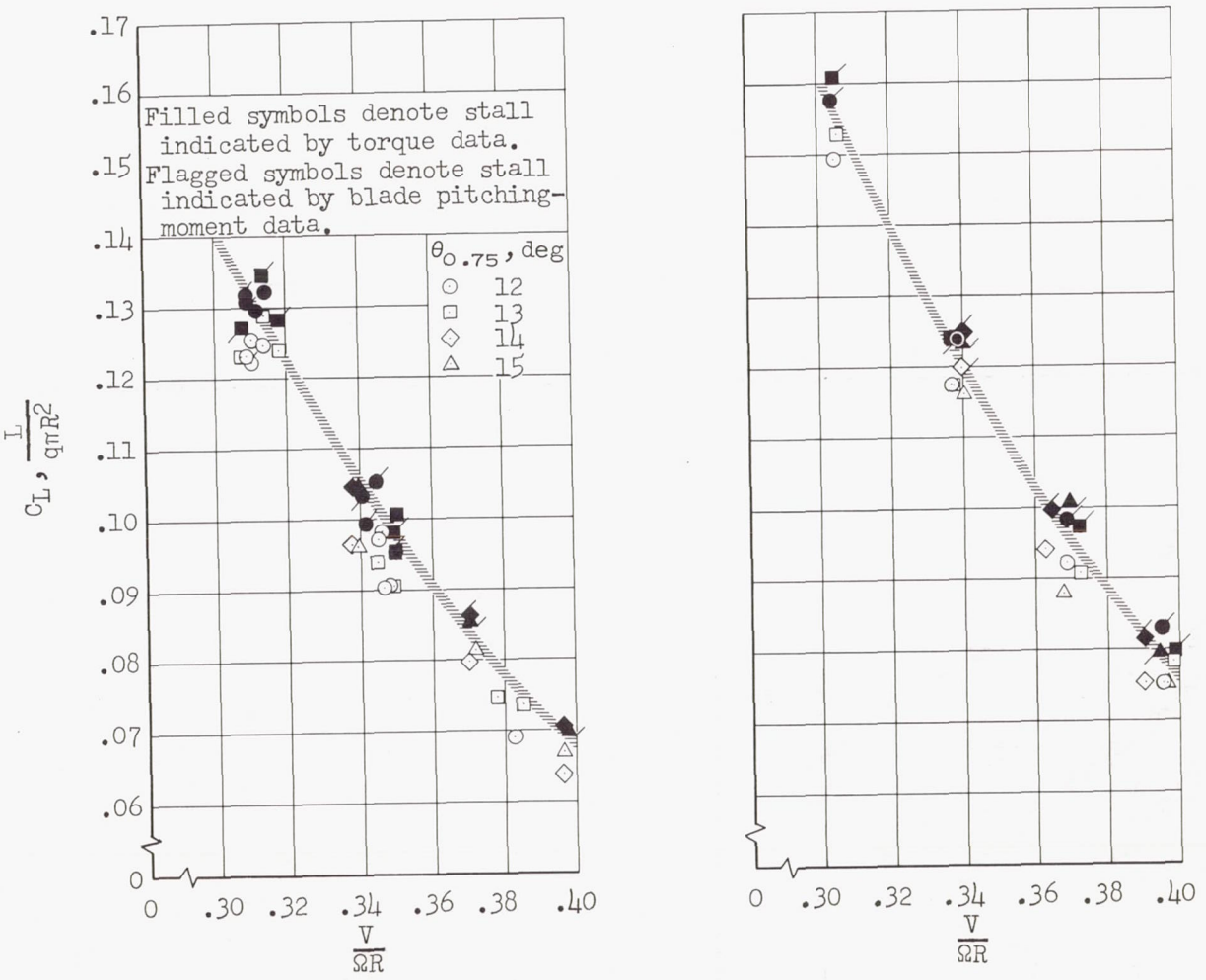

(a) Rotor with symmetrical sections. (b) Rotor with cambered sections.

Figure 10.- Stall boundaries as determined from torque and from blade pitching-moment measurements.

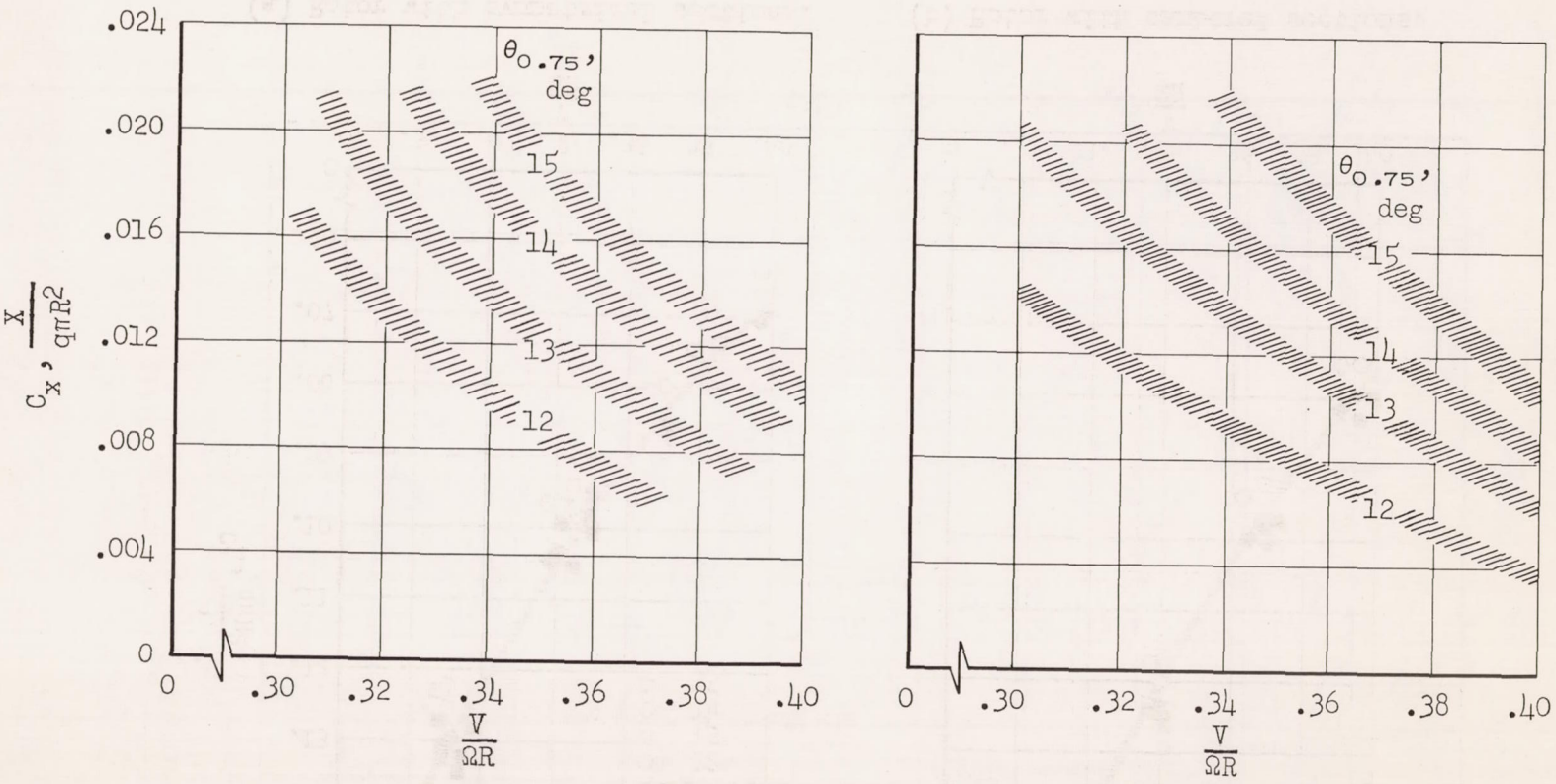

(a) Rotor with symmetrical sections.

(b) Rotor with cambered sections.

Figure 11.- Longitudinal-force coefficient at the stall boundary.

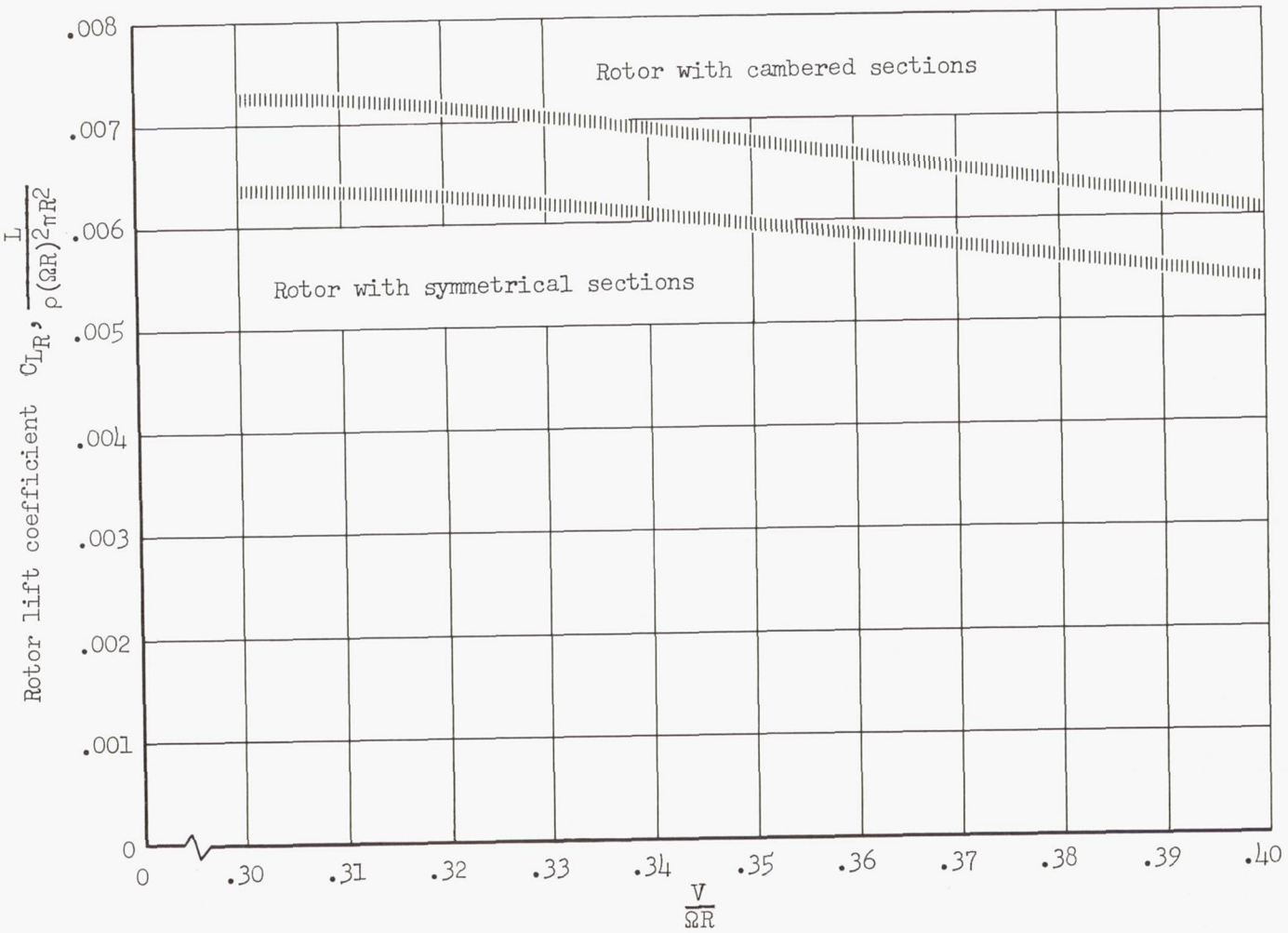

Figure 12.- Comparison of stall boundaries.

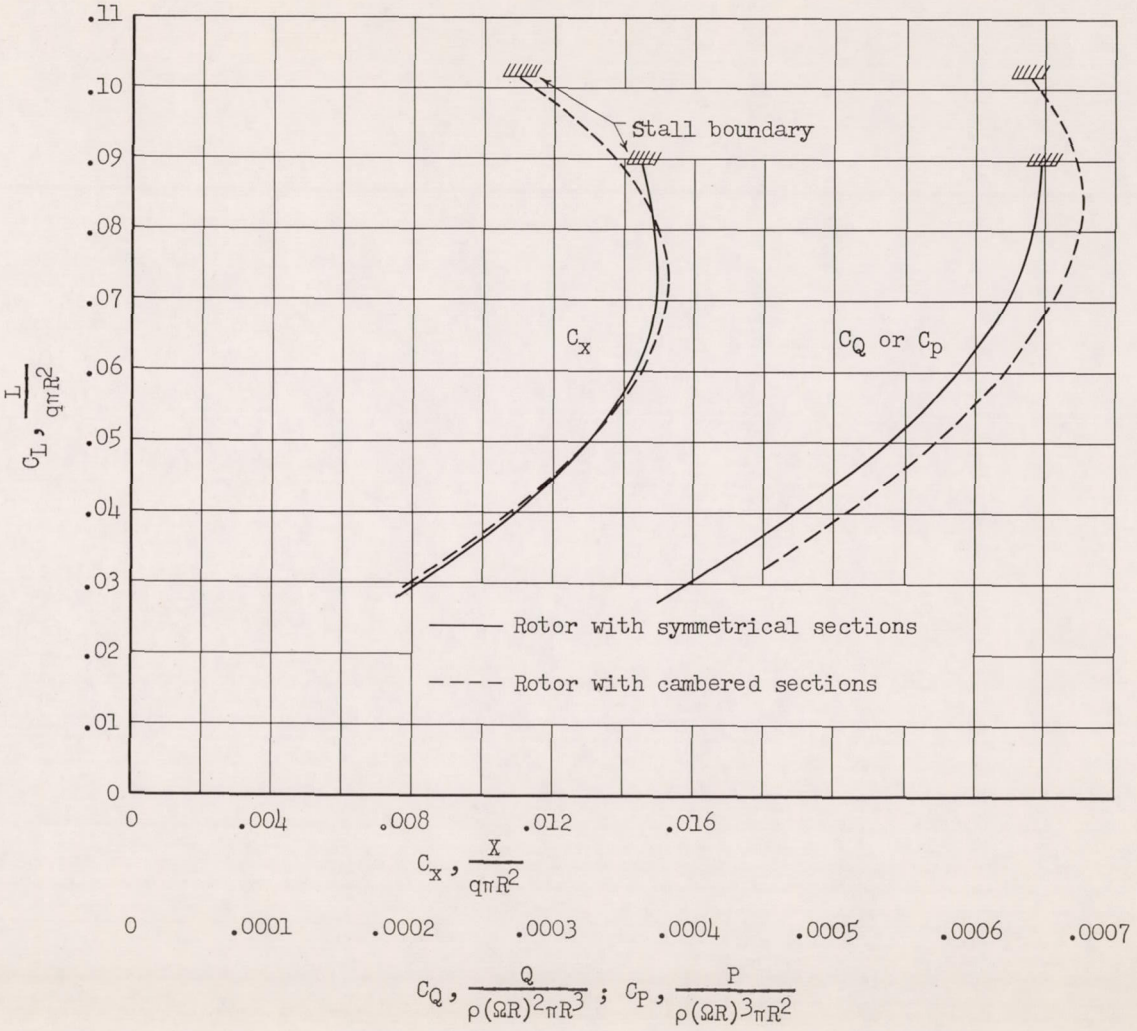

Figure 13.- Comparison of the longitudinal force produced and the power required by the two rotors.

NACA - Langley Field, Va.